In-situ anion exchange with redox mediators influencing the photovoltaic parameters in vacancy-ordered halide perovskite based photoelectrochemical solar cells

Manasa Manoj, [a] Jigar Shaileshkumar Halpati,[a] and Aravind Kumar Chandiran*[a]

Electronic Supplementary information

Experimental Section

Materials.

Cesium bromide (CsBr, 99.9%), cesium iodide (CsI, 99.9%) and Nafion D-521 dispersion (5% w/w in water and 1-propanol) were purchased from Alfa Aesar. Chloroplatinic acid hexahydrate (≥ 37.5% Pt basis) sodium bromide (NaBr, min 99%), lithium iodide (LiI, 99%) and titanium diisopropoxide bis(acetylacetonate) were procured from Sigma Aldrich. Cesium chloride (CsCl, min 99.5%), hydrobromic acid (HBr, ~47% in water) and hydroiodic acid (HI, ~57% aq. solution) were purchased from Spectrochem. Hydrochloric acid (HCl, 35-37%), isopropyl alcohol (IPA, min 99%) from Thermo Fisher Scientific and ethanol from Changshu Hongsheng Fine Chemicals. FTO conducting glass plate (TEC 7 grade) was purchased from Dyesol (Australia).

Material Characterization.

The powder X-ray diffraction pattern of the samples were measured using Rigaku supermini flex 6G with Cu Kα as radiation source in the 2θ range of 10˚ to 60˚ with a step size of 0.1˚/min. High resolution image of the samples were taken using Hitachi S-4800 scanning electron microscopy and the elemental composition and elemental mapping of the samples were obtained using Quanta 200 FEG energy dispersive X-ray spectrometer. Absorption measurement of the samples was collected using Shimadzu 2600 absorption spectrometer equipped with barium sulfate coated integrating sphere. Steady-state photoluminescence measurements were measured using Horiba Fluorolog Spectrofluorometer (Fluorolog-3) containing a 450 W xenon arc lamp with double-excitation monochromator and a single-emission monochromator. A photomultiplier tube detector was used to monitor the photons from the emission monochromator. Emission spectra of the samples were carried out by exciting the samples at 420 nm. Appropriate long-pass cut-off filters were used at the entry port of the emission monochromator to cut off the second order emission peaks. FTIR measurements were carried out using JASCO 6600FV spectrometer with an ATR setup. Measurements were taken from 4000- 50 cm^{-1} where the spectrometer was operated under complete vacuum for far-infrared measurements. Confocal microscopy was carried out for Cs_2PtCl_6 using Leica TCS SP8 with 488nm Argon laser excitation. A 63x lens with oil immersion was used to capture the crystal images. The emission was monitored between 550-750nm by using HyD 3 detector.

Synthesis of Cs_2PtX_6 ($X = Br^-, Cl^-$).

1mmol of CsX ($X = Br^-, Cl^-$) and 0.5 mmol of chloroplatinic acid hexahydrate (>37.5% Pt basis) was added to 3 ml HX ($X = Br^-, Cl^-$) acid in a 50 ml Teflon lined hydrothermal reactor. This reactor was kept in hot air oven for 24 h at 160 °C. After the reaction, it was cooled down to room temperature and the solution was transferred to 15 ml centrifuge tube and centrifuged at 5000 rpm for 10 min and then washed with ethanol to remove any residual solvent. The powder obtained was dried in hot plate at 60 ˚C under vacuum.

Anion exchange.

50 mg of Cs_2PtCl_6 and Cs_2PtBr_6 were added to separate 15ml glass vials. 5 ml 1 M LiI solution made by dissolving LiI in acetonitrile was added to each glass vial. 10 such vials were prepared for studying time dependent exchange of anions where each vial corresponding to each hour. They were kept undisturbed at ambient conditions. After the required time, the solution was taken out and the sample was washed with ethanol and dried at 60 ˚C in hot air oven.

Solar Cell Fabrication

FTO substrate cleaning.

FTO glasses with the area 1.5 x 2 cm^2 were cut out from a 30 x 30 cm^2 FTO glass plate and cleaned by ultrasonicating it in IPA, then in dil. HCl and again in IPA for 20 min. These FTO glasses were heated in hot plate at 500 ˚C for 1 hour.

Photoelectrode

Cleaned and sintered FTO glasses were heated to 450 ˚C and spray pyrolyzed using 1:39 solution of titanium diisopropoxide bis(acetylacetonate) and ethanol. It was then cooled and chemical bath deposition of TiO_2 was carried out by dipping the substrates in 40mM $TiCl_4$ solution in DI water and heated to 75 ˚C in hot air oven for 30 min to form a compact layer of TiO_2. After 30 mins, substrates were taken out and heated on hot plate at 500 ˚C for 45 min. When substrates reach room temperature, perovskite layer is deposited on it.

Film formation.

15 mg of Cs_2PtX_6 (X = Br^-, Cl^-) was added to 200 µl of isopropyl alcohol, 180 µl of DI water and 20 µl of Nafion (5% w/w in water and 1-propanol). This solution was ultrasonicated for 15 mins and 100 µl of the solution was drop-casted onto the prepared FTO and kept undisturbed for drying under ambient conditions. An active area of 0.5 x 0.5 cm^2 was made by scrapping out the remaining area of the film.

Counter electrode

FTOs with an area 1.5 x 2 cm^2 were cut out from the FTO glass plate and holes were drilled for electrolyte injection. It is then cleaned as mentioned above. Platinum coated electrode is prepared by dropping 5 mM solution of H_2PtCl_6 in ethanol on to the sintered FTOs and then kept in a preheated oven at 425 ˚C for 20 mins.

Solar Cells

Photoelectrodes and counter electrodes are melt sealed using Surlyn™ spacers. The electrolyte used was composed of 1M DMII, 50mM LiI, 30mM I_2 and 0.5M *tert*-butyl pyridine in acetonitrile is injected from the opposite side and then vacuum sealed using glue(araldite).

The flat band potential measurements were done using Mott-Schottky technique at a range of applied potentials. To identify the stability window or non-Faradaic region, cyclic voltammetric measurements were carried out in electrolyte (**Figure S17-S18**).

Mechanism of ion-exchange from theoretical perspective

Mechanism of ion exchange processes have also been extensively studied in chalcogenides to enhance the catalytic activity of material. These studies confirm that ion exchange predominantly follows a core-shell mechanism to synthesize intermediate particles, thereby improving the optoelectronic of materials for photovoltaic applications. CdS/PbS, ZnSe/ZnS and PbSe/PbS chalcogenide core and shell nanoplatelets were synthesized through sequential ion exchange.[1] The thickness of the layers can be controlled through the concentration of the solution that provides the ions for conversion. Ethayaraja et al. has carried out theoretical calculations that predicted the model for ion exchange that can be suitable for predicting the thickness or the extend of ion exchange in the crystals.[2]

In systems with negligible interparticle interactions, the ion exchange reaction is governed by diffusion and reaction processes. According to the core-shell mass transfer model, the mechanism involves three sequential steps (**Figure S19**):

(i) **Diffusion** of ions (I^-) from solution to the surface of Cs_2PtCl_6/Cs_2PtBr_6
(ii) **Solid state diffusion** of the anion (I^-) across the surface
(iii) **Anion exchange reaction** where iodide ions (I^-) replace chloride (Cl^-) or bromide (Br^-) ions within their respective materials.

According to Fick's law of mass transfer, the pseudo-steady state diffusion of I^- ions through acetonitrile to $Cs_2Pt(Cl/Br)_6$ crystal can be represented as:

$$J_1 = 4\pi R_0 D_1 (C_B - C_{B,1})$$

where J_1 is the molar diffusion rate of I^- ions, $C_{B,1}$ is the concentration of I^- at the surface of the crystal, and D_1 is the diffusivity of I^- in acetonitrile. Solid state diffusion of I^- through the formed Cs_2PtI_6 shell to the $Cs_2Pt(Cl/Br)_6$ interface can be represented by J_2,

$$J_2 = 4\pi R^2 D_2 \frac{dC_B}{dR}$$

where D_2 is the solid-state diffusivity of I^- in the Cs_2PtI_6 shell. Integrating the above equation w.r.t R using the boundary condition $R = R_0$ at $t = 0$, then

$$J_2 = 4\pi D_2 \frac{RR_0}{R_0 - R}(C_{B,1} - C_{B,2})$$

Where $C_{B,2}$ is the concentration of I^- at the $Cs_2Pt(Cl/Br)_6$ - Cs_2PtI_6 interface. Assuming the reaction to be first order with respect to I- ions, the molar rate of ion exchange reaction (J_3) is given by,

$$J_3 = 4\pi R^2 k_r C_{B,2}$$

Where k_r is the exchange reaction rate constant. At pseudo-steady state, $J_1 = J_2 = J_3$ and the interfacial concentrations $C_{B,1}$ and $C_{B,2}$ can be eliminated. The flux J can be measured in terms of experimental values. On further simplification and integration w.r.t time, an analytical solution can be obtained that will give the characteristic time constant for the complete conversion. It has to be noted that the core/shell structure assumed a spherical morphology in the mathematical model. The diffusion of iodide from the electrolyte and the exchange of iodide with chloride/bromide might not be a rate limiting step, compared to the diffusion of iodide in the shell of Cs_2PtI_6 towards the core. So J_2 would be the determining factor for the anion exchange reaction. This explanation corroborates with the

XRD data, wherein the Cs_2PtCl_6/Cs_2PtBr_6 diminishes in first 3-4 hours with significant increase in Cs_2PtI_6 phase. However, the complete conversion to iodide phase took another 6 to 7 hours, possibly because of slow iodide (solid-state) diffusion through the shell (Cs_2PtI_6) towards the core (Cs_2PtCl_6/Cs_2PtBr_6). This trend can be observed only in core-shell structures. Assuming the formation for Cs_2PtI_6 via decomposition of parent material (Cs_2PtCl_6/Cs_2PtBr_6) and recrystallization with iodide anion, the core of Cl/Br noted in SEM couldn't be observed. The mechanism of solid-state diffusion of iodide ion is illustrated in few research articles. Julian et al. provided insights into ion movement through molecular dynamics simulations. It was proposed that diffusion occurs via a halide vacancy-mediated mechanism. The computed halide vacancy formation free energies are relatively low, resulting in high equilibrium vacancy concentrations that enable significant inter-diffusivity. Anions overcome free energy barriers by exchanging positions with vacancies, and intrinsic ion diffusion is facilitated by the soft lattice structure of halide perovskites. This soft lattice reduces vacancy hopping barriers, as revealed through molecular dynamics simulations, thereby promoting efficient ion exchange. [3,4]

The predicted formation energies of Cs_2PtCl_6, Cs_2PtBr_6, Cs_2PtI_6 are -1.433 eV/atom, -1.233 eV/atom and -0.971 eV/atom respectively.[5–7] Higher formation energy indicates lower stability, however here the anion exchange is driven by local conditions such as interaction of halide ion with the host lattice and halide ion concentration in the solution. The halogen X-site has the lowest activation energy among the A and B site ions due to the halide vacancy assisted diffusion. The halide vacancies induces strain in the material.[8] The I^- ions have a larger ionic radius than Cl^- and Br^-, leading to a lattice expansion that relieves the strain.[9–11] Due to this halide perovskites are subjected to anion exchange irrespective of the bond strength. Kovalenko et al. and Manna et al. independently demonstrated fast anion exchange from Cl → Br, Br → I and Cl → I by adjusting the halide ratios in the halogen precursor source.[12,13] Moreover, the anion exchange is driven by chemical potential gradient of halides. The chemical potential gradient of halide ions in the electrolyte is higher than that of halides in the perovskite structure thereby driving the diffusion of the halides.

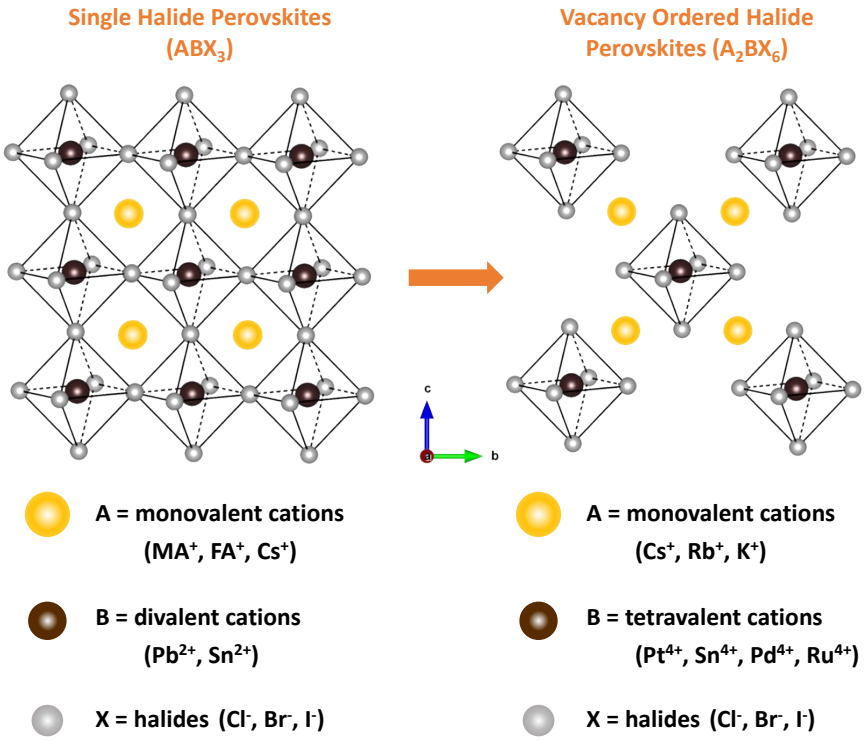

Figure S1. Crystal structure representation of conventional halide perovskites and vacancy ordered halide perovskites. (MA-methyl ammonium, FA-formamidinium)

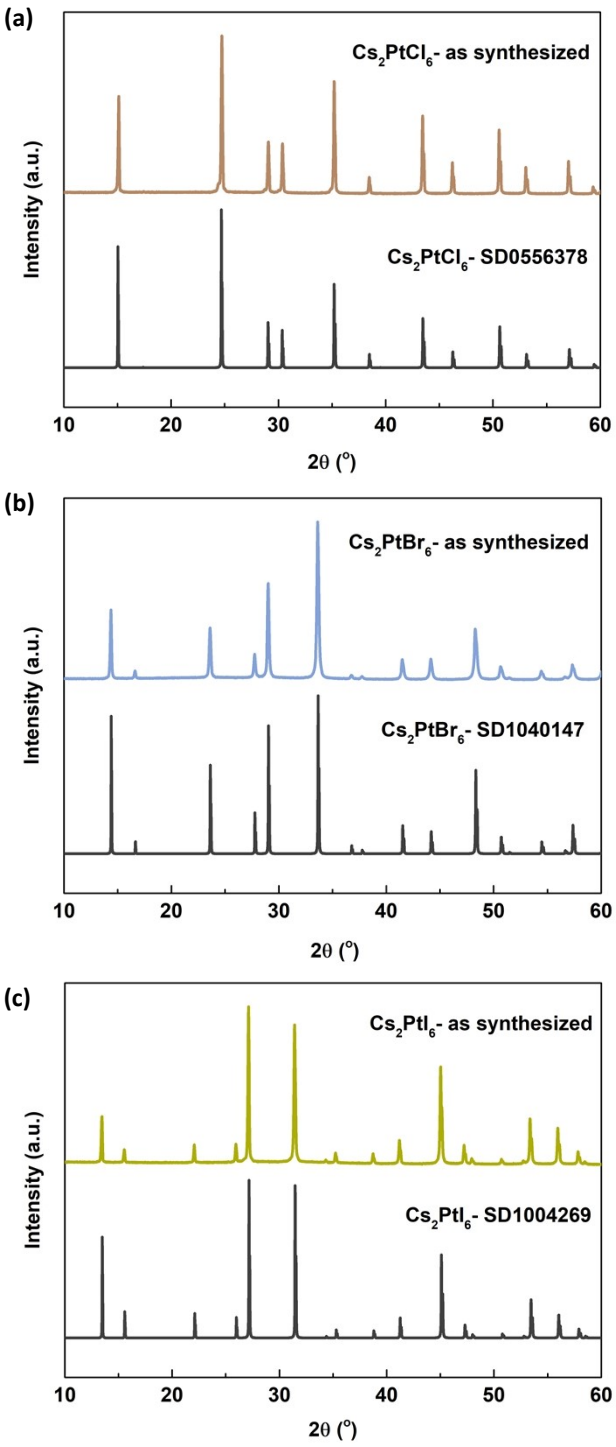

Figure S2. XRD comparison of the as-synthesized material with the literature

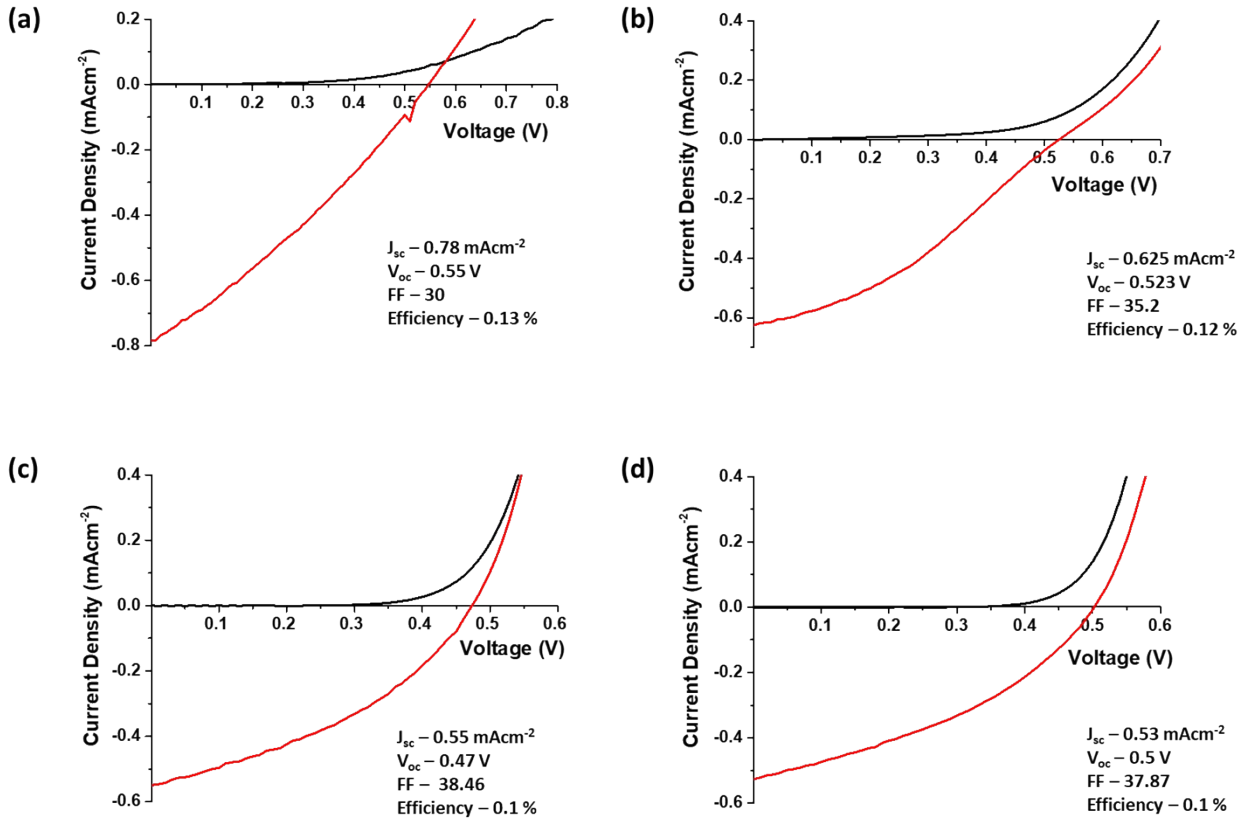

Figure S3. J-V characterization of Cs_2PtCl_6 within the same efficiency range as the champion cell

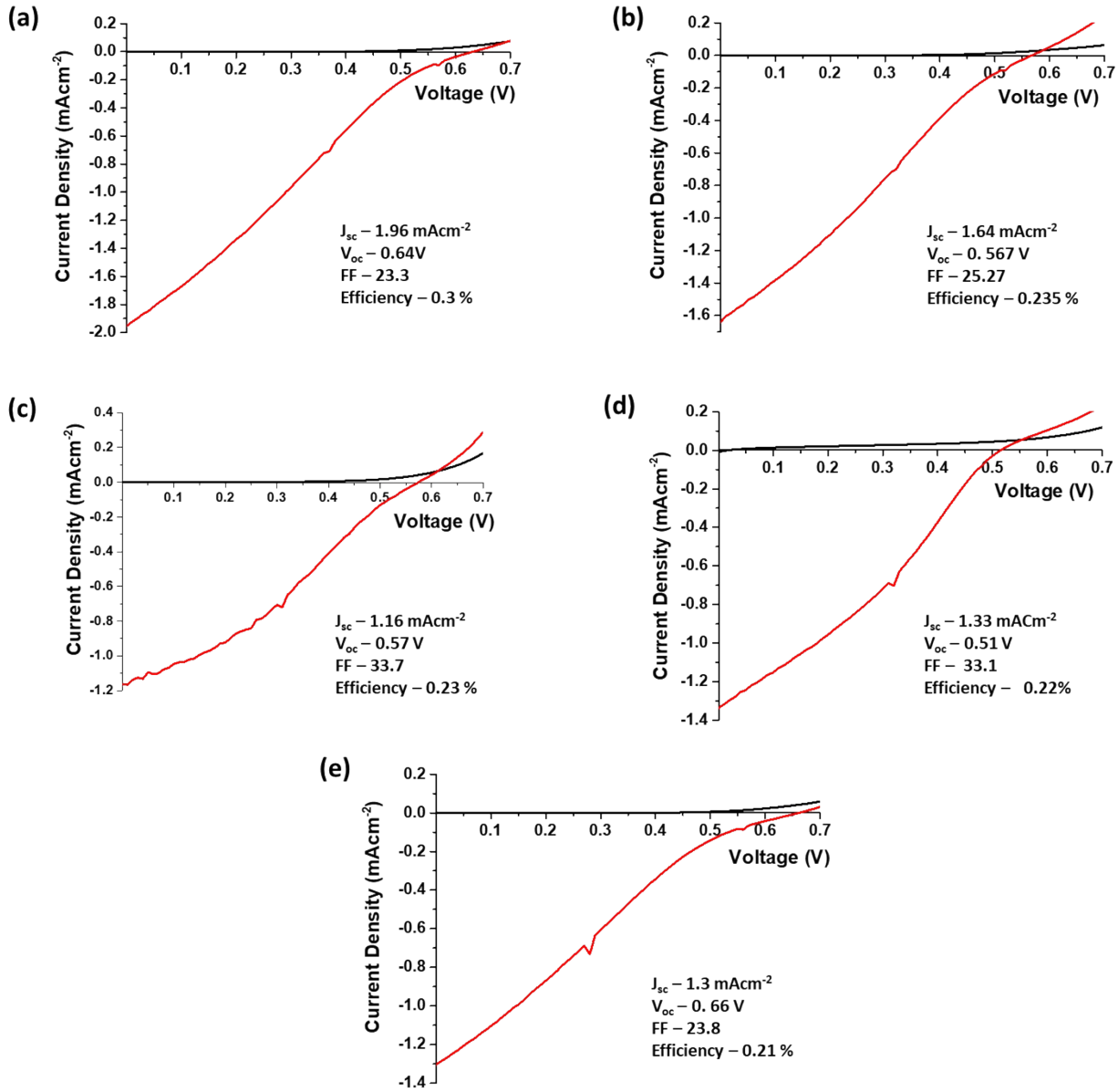

Figure S4. J-V characterization of Cs_2PtBr_6 within the same efficiency range as the champion cell

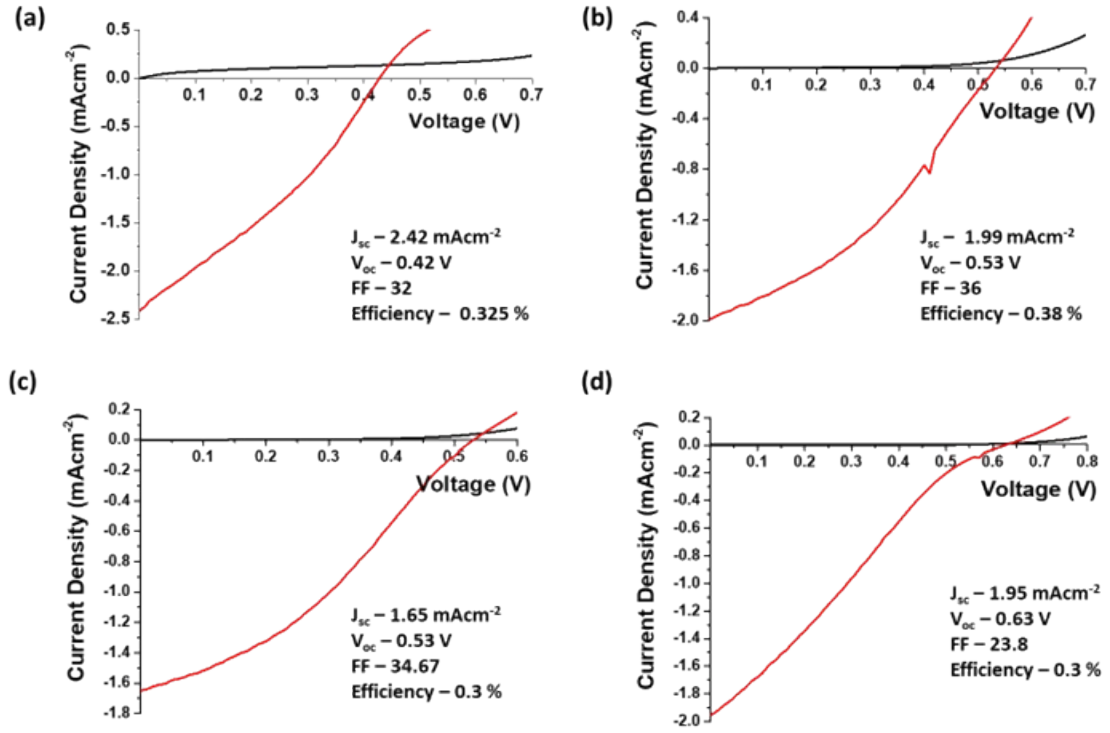

Figure S5. J-V characterization of Cs_2PtI_6 within the same efficiency range as the champion cell

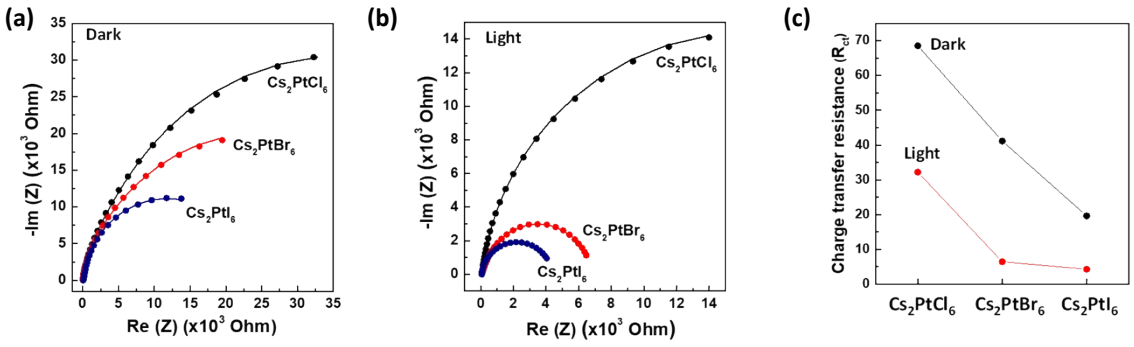

Figure S6. (a)-(b) Impedance spectra of Cs_2PtX_6 under dark and light conditions, respectively. **(c)** Variation in charge transfer resistance for Cs_2PtX_6 under dark and light conditions.

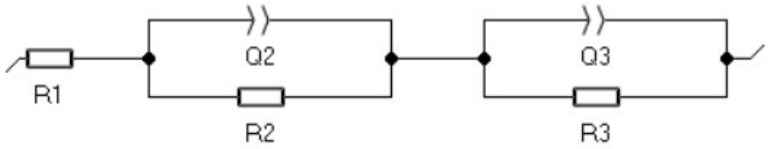

Figure S7. The equivalent circuit used for fitting the electrochemical impedance data of solar cell in light and dark conditions

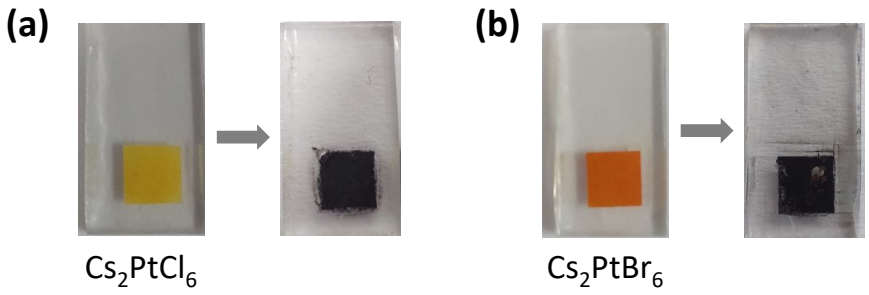

Figure S8. Colour change of **(a)** Cs_2PtCl_6 and **(b)** Cs_2PtBr_6 to black

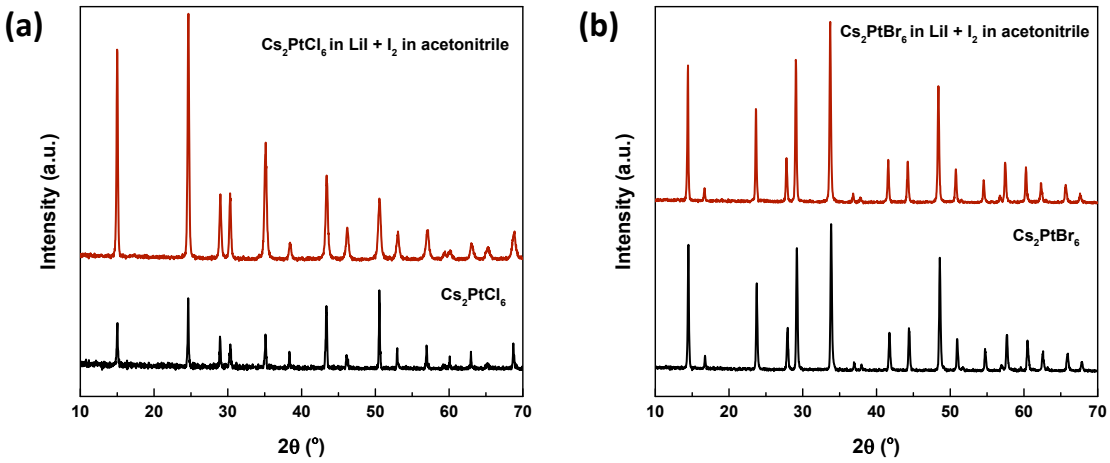

Figure S9. (a) Stability of Cs_2PtCl_6 in LiI + iodine in acetonitrile **(b)** Stability of Cs_2PtBr_6 in LiI + iodine in acetonitrile

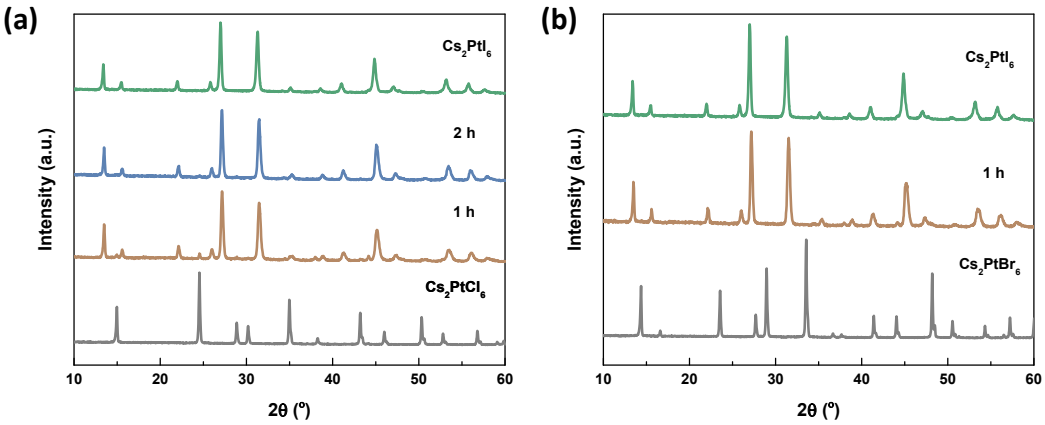

Figure S10. Anion exchange of **(a)** Cs_2PtCl_6 **(b)** Cs_2PtBr_6 to Cs_2PtI_6 in lithium iodide solution at 60 °C

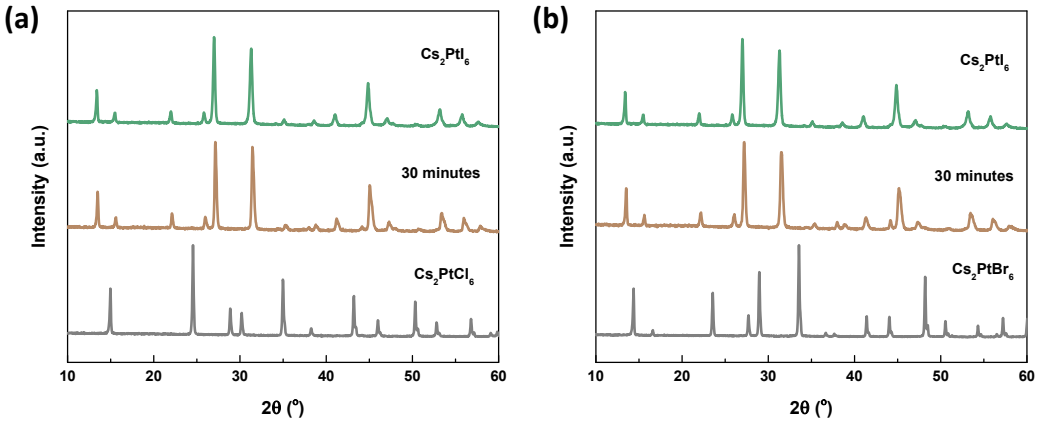

Figure S11. Anion exchange of **(a)** Cs_2PtCl_6 **(b)** Cs_2PtBr_6 to Cs_2PtI_6 in lithium iodide solution at 100 °C

When the anion exchange reaction was carried out at room temperature (30 °C), the conversion took 10 hours to complete whereas when the temperature is increased to 60 °C, the conversion completed in a shorter period of time. From the X-ray diffraction pattern in **Figure S10**, it can be observed that Cs_2PtCl_6 took 2 hours for completion and Cs_2PtBr_6 took 1 hours for complete conversion to Cs_2PtI_6. Similarly, when the temperature was elevated to 100 °C, both the materials converted to Cs_2PtI_6 in less than 30 minutes according to **Figure S11**.

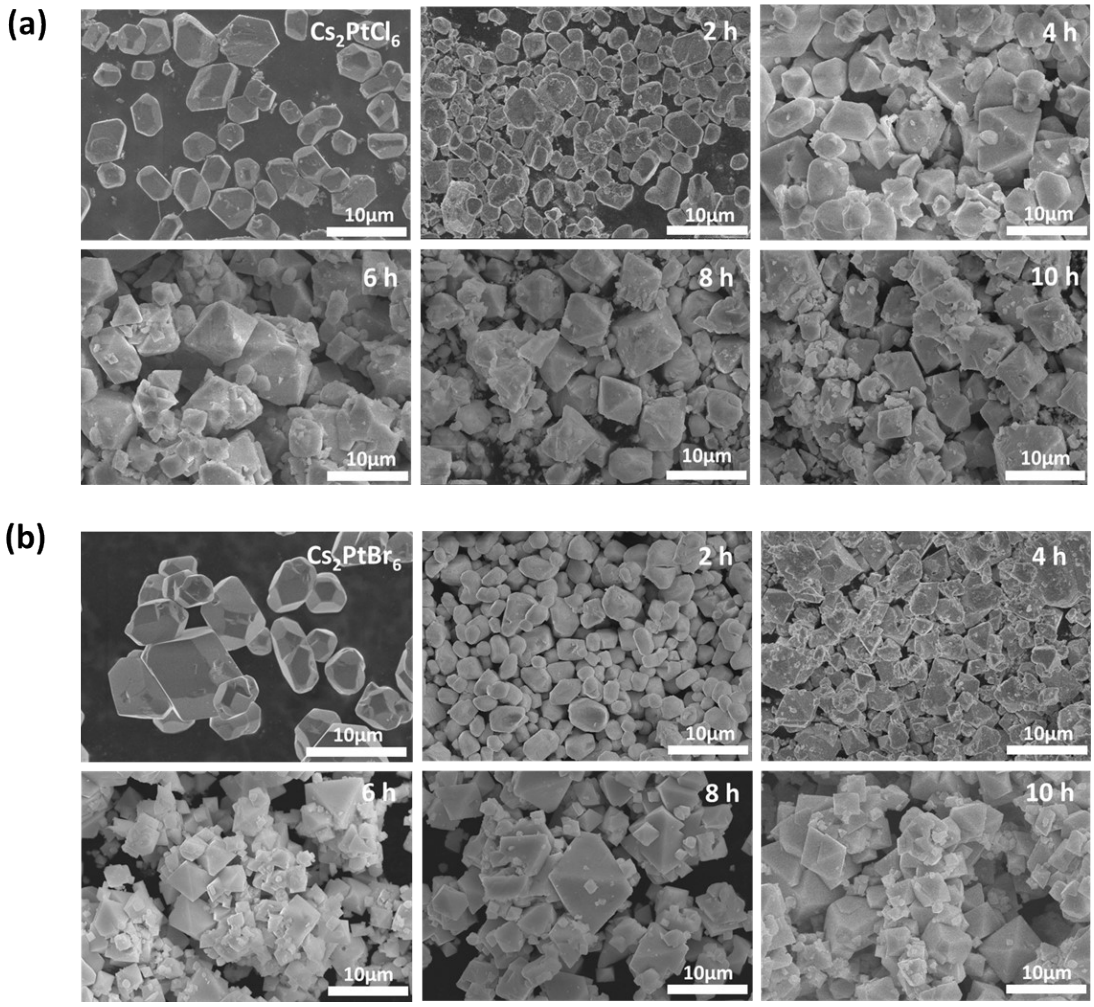

Figure S12. SEM micrographs of Cs_2PtCl_6 **(b)** Cs_2PtBr_6, dispersed in LiI solution as a function of time.

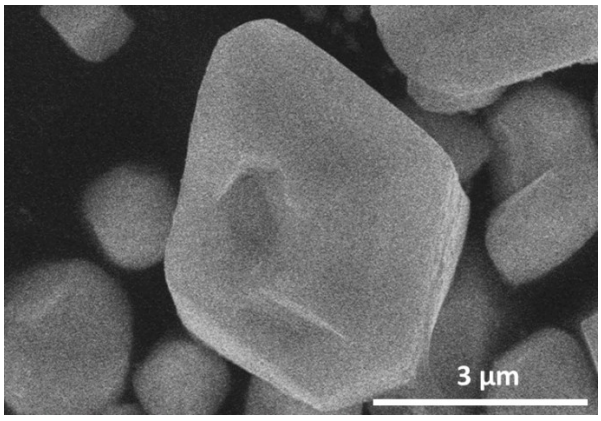

Figure S13. SEM micrograph of Cs_2PtI_6

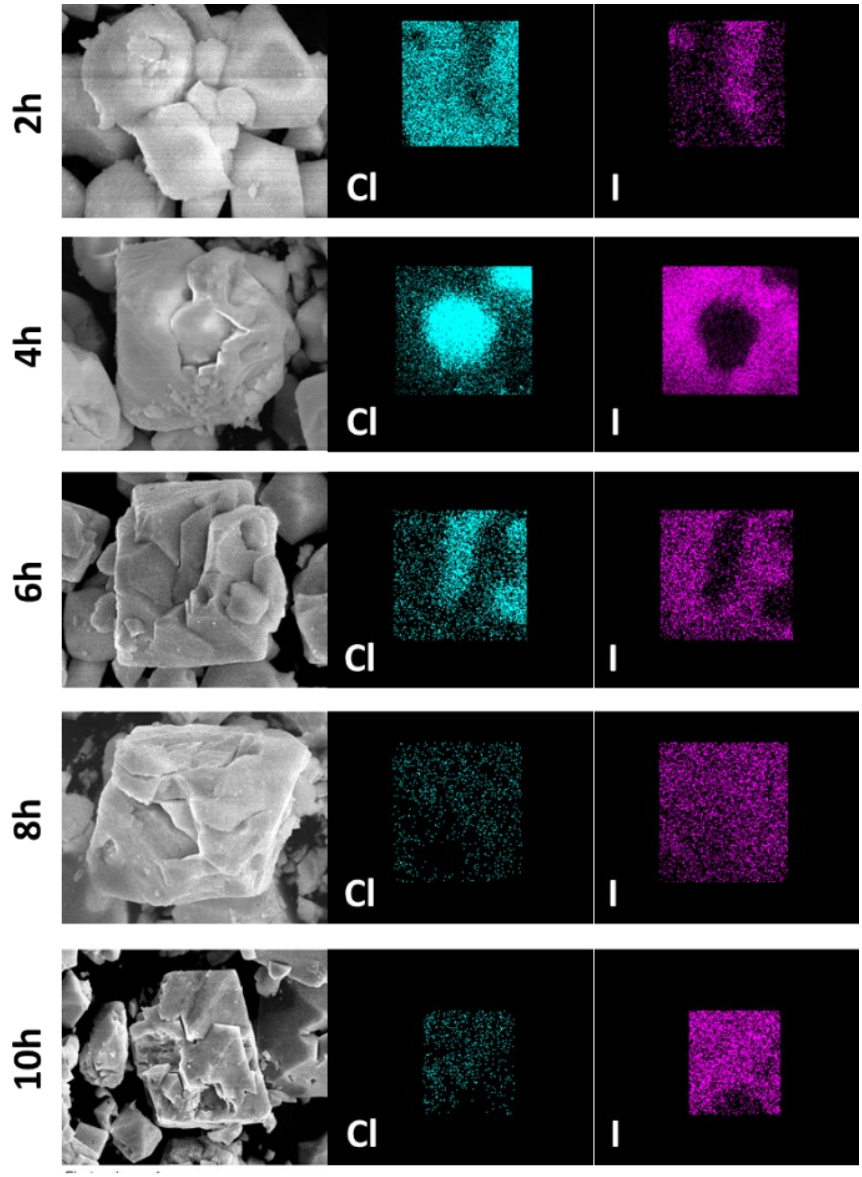

Figure S14. Elemental mapping of Cs_2PtCl_6 with time where chloride ions in the shell is slowly replaced by iodide ions

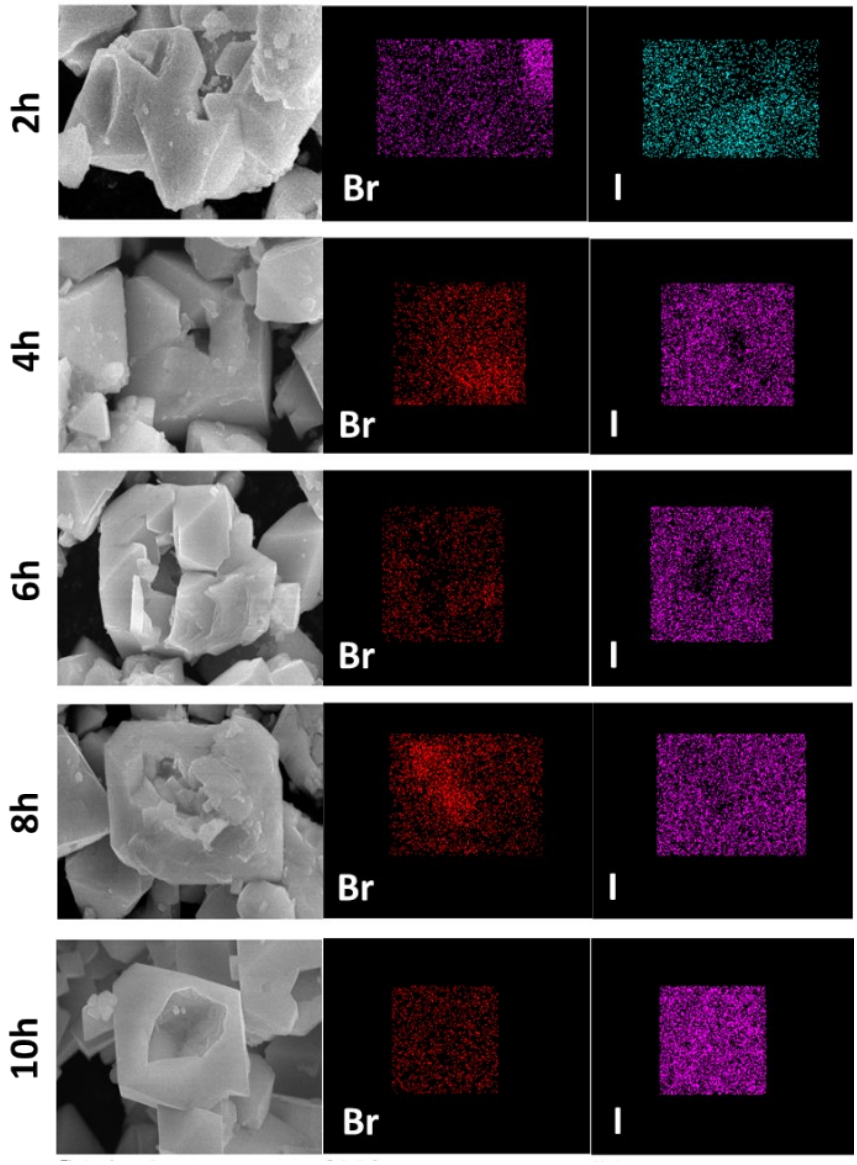

Figure S15. Elemental mapping of Cs_2PtBr_6 with time where bromide ions in the shell is slowly replaced by iodide ions

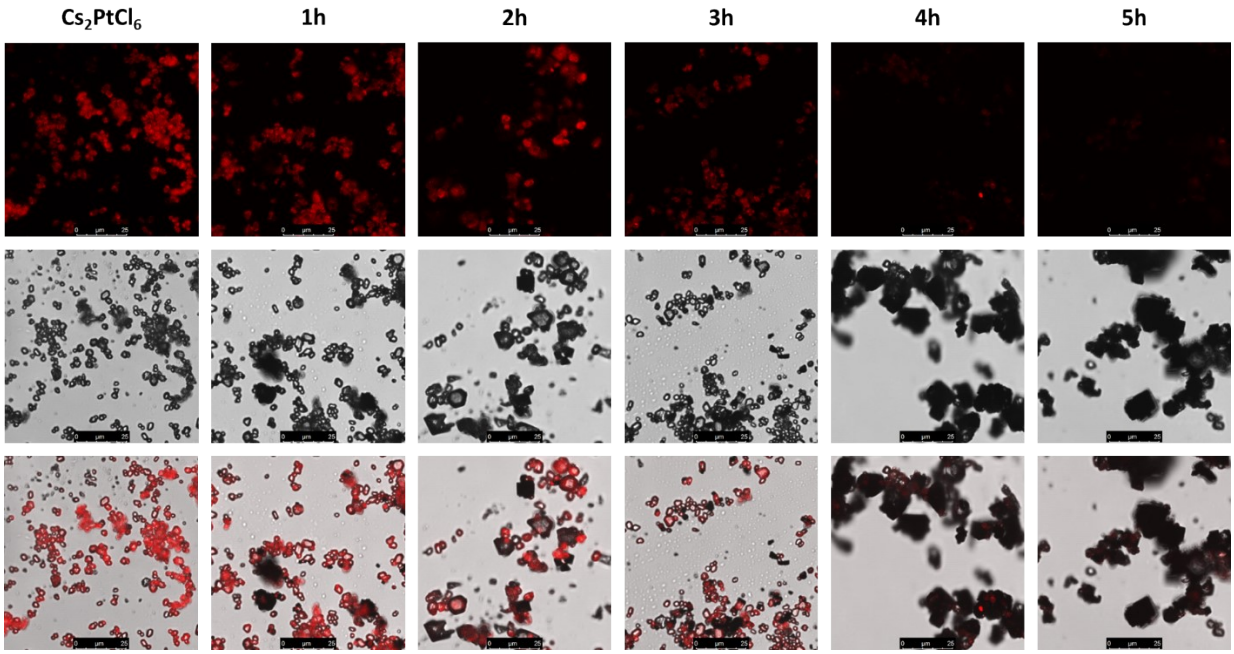

Figure S16. Confocal imaging of Cs_2PtCl_6. With time the emission is quenched due to the formation of Cs_2PtI_6. After 3 hours, emission quenched drastically which aligns with the emission spectra. Top panel shows PL images, middle panel shows transmission images and the bottom panel provides the overlap of these two. The overlap images show that black outer surface.

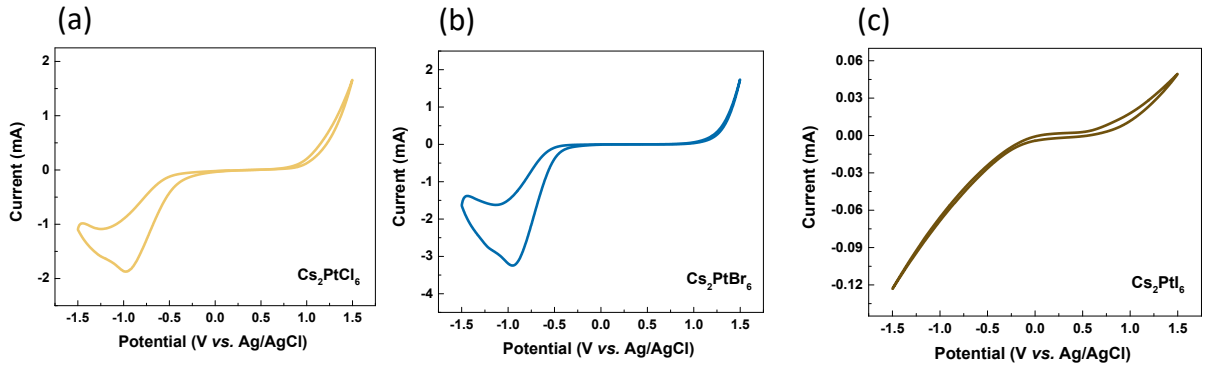

Figure S17. Cyclic voltammogram of **(a)** Cs_2PtCl_6, **(b)** Cs_2PtBr_6, and **(c)** Cs_2PtI_6 in iodide/triiodide electrolyte to find the stable electrochemical window for Mott-Schottky measurements.

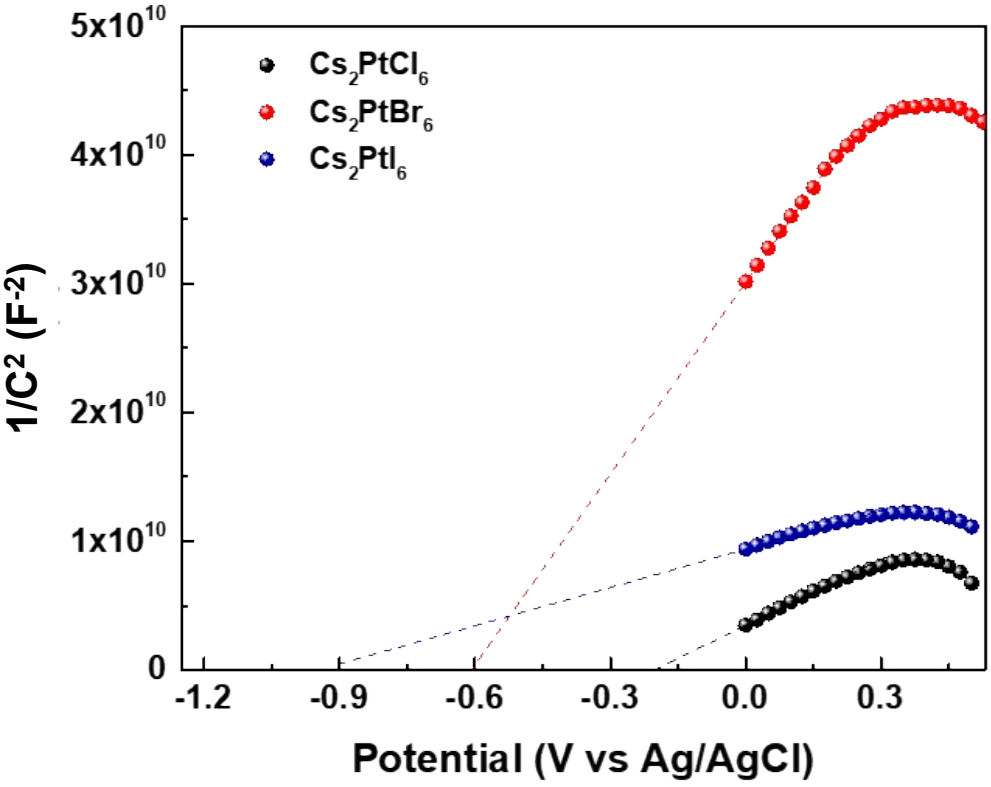

Figure S18. Mott-Schottky measurements to identify the flat band potential

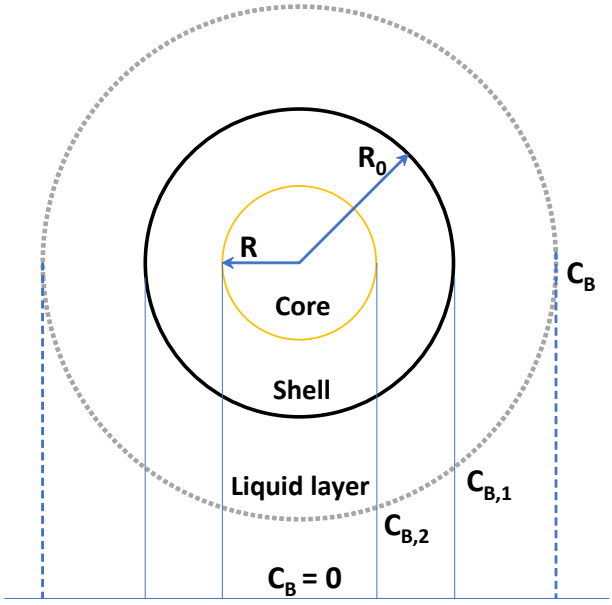

Figure S19. Pseudo-steady state concentration profile of I^- ions across the crystal

Table S1. Summary of efficiency data for selected set of PEC solar cells.

Sr. no.	Photoanode assembly	Electrolyte/HTM	Efficiency	Ref
1.	Dropcasted-TiO_2|$CH_3NH_3PbI_3$	I^-/I_3^-	3.81%	[14]
2.	Spin-coated-TiO_2|$CH_3NH_3PbI_3$	I^-/I_3^-	6.54%	[15]
3.	TiO_2|CdS/CdSe-QDs	1M Na_2S, 0.1 M S, 0.2 M KCl	3.4%	[16]
4.	TiO_2|CdS/Mn:CdSe-QDs	1M Na_2S, 0.1 M S, 0.2 M KCl	4.9%	[16]
5.	$BaSnO_3$|$BaSnO_3$ + N719	I^-/I_3^-	6.2%	[17]
6.	TiO_2|$CuInS_2$-QDs	1.8 M Na_2S, 2 M sulfur, 0.2 M KCl	1.27%	[18]

Table S2. Fit data of EIS

Condition	Photo-absorber	R1 (Ω)	R2 (Ω)	Q2 (x 10^{-6} F)	R3 (Ω)	Q3 (x 10^{-6} F)	Total resistance (Ω)
Dark	Cs_2PtCl_6	71.74	10575	8	57896	3.53	68542
	Cs_2PtBr_6	59.44	7238	7.55	33858	3.81	41155
	Cs_2PtI_6	58.42	3392	9.23	18183	0.147	21633
Light	Cs_2PtCl_6	53.77	5301	4.08	26854	0.775	32208
	Cs_2PtBr_6	34.17	1214	9.85	5272	0.699	6452
	Cs_2PtI_6	24.22	868	8.33	3401	0.130	4293

References

1 C. Bouet, D. Laufer, B. Mahler, B. Nadal, H. Heuclin, S. Pedetti, G. Patriarche and B. Dubertret, *Chem. Mater.*, 2014, **26**, 3002–3008.

2 M. Ethayaraja and R. Bandyopadhyaya, *Ind. Eng. Chem. Res.*, 2008, **47**, 5982–5985.

3 B. A. Koscher, N. D. Bronstein, J. H. Olshansky, Y. Bekenstein and A. P. Alivisatos, *J. Am. Chem. Soc.*, 2016, **138**, 12065–12068.

4 J. A. Steele, M. Lai, Y. Zhang, Z. Lin, J. Hofkens, M. B. J. Roeffaers and P. Yang, *Acc. Mater. Res.*, 2020, **1**, 3–15.

5 Materials Data on Cs2PtBr6 by Materials Project, 2020. https://doi.org/10.17188/1204490, 2020.

6 Materials Data on Cs2PtCl6 by Materials Project, 2020. https://doi.org/10.17188/1199485, 2020.

7 Materials Data on Cs2PtI6 by Materials Project, 2020. https://doi.org/10.17188/1199206, 2020.

8 Y. W. Woo, Y.-K. Jung, G. Y. Kim, S. Kim and A. Walsh, *Discover Materials*, 2022, **2**, 8.

9 Y. Marcus, *Chem. Rev.*, 1988, **88**, 1475–1498.

10 C. Eames, J. M. Frost, P. R. F. Barnes, B. C. O'Regan, A. Walsh and M. S. Islam, *Nature Communications*, 2015, **6**, 7497.

11 R. D. Shannon, *Acta Cryst A*, 1976, **32**, 751–767.

12 G. Nedelcu, L. Protesescu, S. Yakunin, M. I. Bodnarchuk, M. J. Grotevent and M. V. Kovalenko, *Nano Lett.*, 2015, **15**, 5635–5640.

13 Q. A. Akkerman, V. D'Innocenzo, S. Accornero, A. Scarpellini, A. Petrozza, M. Prato and L. Manna, *J. Am. Chem. Soc.*, 2015, **137**, 10276–10281.

14 A. Kojima, K. Teshima, Y. Shirai and T. Miyasaka, *J. Am. Chem. Soc.*, 2009, **131**, 6050–6051.

15 J.-H. Im, C.-R. Lee, J.-W. Lee, S.-W. Park and N.-G. Park, *Nanoscale*, 2011, **3**, 4088–4093.

16 C. Zhang, S. Liu, X. Liu, F. Deng, Y. Xiong and F.-C. Tsai, *Royal Society Open Science*, 2018, **5**, 171712.

17 S. S. Shin, J. S. Kim, J. H. Suk, K. D. Lee, D. W. Kim, J. H. Park, I. S. Cho, K. S. Hong and J. Y. Kim, *ACS Nano*, 2013, **7**, 1027–1035.

18 C.-C. Chang, J.-K. Chen, C.-P. Chen, C.-H. Yang and J.-Y. Chang, *ACS Appl. Mater. Interfaces*, 2013, **5**, 11296–11306.